ChemSusChem
Chemistry–Sustainability–Energy–Materials
Chemistry Europe
European Chemical Societies Publishing

Volume 14, Issue 8
April 22, 2021
Pages 1902-1912

Full Paper

Structure–Reactivity Effects of Biomass-based Hydroxyacids for Sustainable Electrochemical Hydrogen Production

Dr. Daniel Martín-Yerga, Jai White, Prof. Gunnar Henriksson, Prof. Ann Cornell

First published: 17 February 2021 | https://doi.org/10.1002/cssc.202100073

Structure-reactivity effects of biomass-based hydroxyacids for sustainable electrochemical hydrogen production

Dr. Daniel Martín-Yerga[a,c]*, Jai White[a], Prof. Gunnar Henriksson[b], Prof. Ann Cornell[a]*

[a]*Department of Chemical Engineering, KTH Royal Institute of Technology, SE-100 44 Stockholm, Sweden*

[b]*Department of Fibre and Polymer Technology, KTH Royal Institute of Technology, SE-100 44 Stockholm, Sweden*

[c] Current address: *Department of Chemistry, University of Warwick, Coventry CV47AL, United Kingdom.*

***Corresponding authors' e-mail:**

D.M-Y daniel.martin-yerga@warwick.ac.uk

A. C amco@kth.se

ABSTRACT

Biomass electro-oxidation is a promising approach for the sustainable generation of H_2 by electrolysis with simultaneous synthesis of value-added chemicals. In this work, we comparatively study the electro-oxidation of two structurally-different organic hydroxyacids, lactic acid and gluconic acid, to understand how the chemical structure of the hydroxyacid affects the electrochemical reactivity under various conditions. We conclude that hydroxyacids such as gluconic acid, with a considerable density of C-OH groups, are highly reactive and promising for the sustainable generation of H_2 by electrolysis at low potentials and high conversion rates (less than -0.15 V vs Hg/HgO at 400 mA cm^{-2}) but with low selectivity to specific final products. In contrast, the lower reactivity of lactic acid did not enable H_2 generation at very high conversion rates (< 100 mA cm^{-2}) but the reaction was significantly more selective (64% to pyruvic acid). This work shows the potential of biomass-based organic hydroxyacids for sustainable generation of H_2 and highlights the importance of the chemical structure on the reactivity and selectivity of the electro-oxidation reactions.

KEYWORDS: Biomass valorization; Electrocatalysis; Electrochemistry; Energy conversion; Hydrogen production.

INTRODUCTION

The energy and industrial systems worldwide require a substantial transformation to overcome current societal challenges such as global warming and the shortage of fossil-based feedstocks.[1] Development of greener and more sustainable alternatives to current energy technologies is the way forward to solve those issues. Hydrogen is expected to become a key component as clean fuel and its use is predicted to significantly increase in the near future from applications such as electricity generation by fuel cells, replacement of coke for iron ore reduction in the steel industry, hydrogenation of biomass components in fuel manufacturing and the replacement of natural gas as the hydrogen source in a sustainable Haber-Bosch process for ammonia, and thereby for fertilizer production.[2,3]

Electrolysis through water splitting represents a clean and sustainable production of H_2,[4,5] particularly if the electricity comes from renewable sources such as wind or solar. In water splitting, water is reduced at the cathode electrode to generate H_2 through the hydrogen evolution reaction (HER) while it is oxidized at the anode electrode through the oxygen evolution reaction (OER) as represented in Figure 1a. The main challenge of this technology is the high thermodynamic potential and sluggish kinetics of the OER, which makes the overall H_2 production a quite energy-intensive process with current technologies requiring between 35-55 kWh kg^{-1} H_2.[5] Replacing the OER by another oxidation reaction with a lower thermodynamic potential is a common option to decrease the energy requirements for H_2 production. In this regard, electro-oxidation of biomass-based chemicals has attracted a significant interest for H_2 production in recent years,[6,7] usually requiring less energy than water splitting (18-20 kWh kg^{-1} H_2),[8] and with the extra advantage of simultaneously producing other valuable chemicals (Figure 1b) from sustainable and low-value biomass feedstocks,[9] which is the main objective of modern bio-refineries.[10–12] Large scale production of hydrogen by electrolysis should thus gain from low cost biomass-based chemicals available in large amounts. Alcohols such as methanol,[13,14]

ethanol[15,16] and glycerol,[17] which can be obtained from biomass sources, are easily oxidized and have been the target of numerous research studies to be used as the anodic reaction for electrolytic production of H_2. One source for such alcohols is degradation products, the black liquor, from polysaccharides in alkaline chemical pulping of wood. However, components from these biomass sources do often contain a carboxylic acid in addition to the alcohol groups (called organic hydroxyacids or sugar acids),[18,19] which might affect the reactivity compared to the well-studied alcohol electro-oxidation and, thus, the performance for sustainable H_2 production.

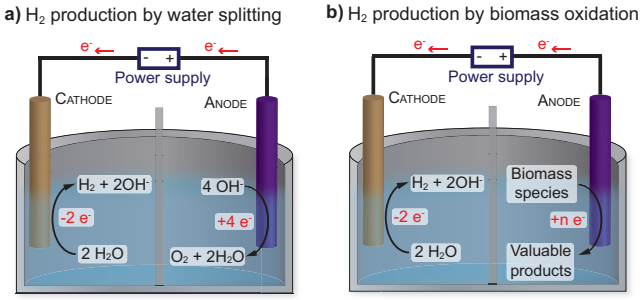

Figure 1. Schematic of H_2 production by electrolysis from a) water splitting and b) biomass oxidation.

Lactic acid (LA), a hydroxyacid widely found in biomass feedstocks or produced from them,[20] such as in black liquor,[19] has been selected as one of the top 15 platform chemicals from biorefinery carbohydrates by the US Department of Energy[21] as it can be converted into a wide range of useful intermediates,[20,22,23] such as pyruvic acid,[24] a potential precursor for many chemicals, pharmaceuticals, food additives and polymers.[11,20,25] The classical production route of pyruvic acid is the chemical dehydration and decarboxylation of tartaric acid,[26] a method developed by Erlenmeyer in 1881. However, this method consumes a large (stoichiometric) amount of $KHSO_4$ and energy (the reaction is performed at around 300 ºC) leading to a cost-ineffective and wasteful process, which makes the development of greener and cost-effective production routes for pyruvic acid of great importance. For instance, electrochemical oxidation of LA could be an interesting alternative and several studies have been previously reported. LA oxidation in acidic media has been studied with Pt-based electrodes,[27,28] where a mechanism

through the reaction of LA with electrogenerated hydroxyl radicals at high anodic potentials as a result of water oxidation was proposed. Initial formation of pyruvic acid was reported but the final products were mainly acetic acid or CO_2.[27] Yuksel et al. reported the electro-oxidation of LA in alkaline media at subcritical conditions (10 MPa, 280 ºC) using titanium electrodes.[29] Under these conditions, acetaldehyde was the main product (~25 %), with an overall conversion of 55%. Acrylic and acetic acids were also detected but at lower yields (1-2%). In another report, an iridium oxide catalyst was employed for LA electro-oxidation in acidic media.[30] In this case, the objective was to remove LA from wastewater, which mainly led to the formation of CO_2 (89% selectivity), but at the expense of applying a very high potential (+2.7 V vs the standard hydrogen electrode, SHE). A recent study has reported the production of pyruvic acid by electrolysis of LA from a fermentation broth in alkaline media and co-production of H_2 at the cathode.[31] However, this method has several drawbacks such as the application of a very high cell potential (+5.0 V), demonstrating a very low performance in terms of energy requirements. The method achieved a selectivity of 58% to pyruvic acid with a significant amount of acetaldehyde (16%) also produced. Authors observed O_2 bubbles at the anode as expected at those high potentials, which suggests that the LA oxidation was indirect through reacting with *in situ* electro-generated hydroxyl radicals. In contrast, we have recently reported an interesting approach to achieve the LA oxidation at low potentials with good selectivity to pyruvic acid (88%) using a PdNi electrocatalyst.[32] The applied potential was modulated as a function of time to achieve an *in situ* reactivation of the catalyst, which ~~allowed an enhancement of~~ enhanced the H_2 production rate compared to conventional galvano- or potentiostatic methods. However, the current densities recorded during LA oxidation were still low for its successful application to large scale H_2 production. Therefore, there is still room for improvement to develop strategies for high-performance LA electro-oxidation with good selectivity to valuable products and simultaneous production of H_2 at considerable rates which might be applicable to industrial settings.

Another characteristic organic hydroxyacid is gluconic acid (GA),[33] which is conventionally produced by glucose fermentation[34] but also by more economical approaches such as oxidation of glucose[35,36] or cellobiose[37,38] by heterogeneous catalysis. It is also a good representative of sugar degradation products present in black liquor. GA is mainly used in the food industry as an acidity regulator,[33] but it might become a promising sustainable and cost-effective platform chemical to produce an additional range of chemicals such as tartaric, oxalic or glucaric acids for further applications, with the latter being considered as one of the most valued chemical products that can be derived from biomass.[39] Whilst the valorization of GA by heterogeneous catalysis seems to be a promising and well-investigated application,[40] it is still unknown if this hydroxyacid could become a good option for the sustainable production of H_2 by electrolysis since only a few and very limited studies regarding the electro-oxidation of GA have been reported. For instance, GA electro-oxidation on graphite electrodes has shown to produce arabinose with good selectivity,[41,42] but the lack of electrocatalytic properties of graphite required the application of a very high potential (+1.5 V vs SHE). Moggia et al. studied the oxidation of glucose and several hydroxyacids such as gluconic, glucaric and glucuronic acids on Cu, Au and Pt electrodes.[39] The oxidation potential for GA was significantly lower on Au and Pt than on Cu electrodes, suggesting that good electrocatalytic properties such as the ones provided by noble metals are required to achieve the GA electro-oxidation at low potentials, which is desirable in terms of energy requirements for H_2 production at a larger scale. However, this study was very limited in terms of practical application, the product selectivity was not reported and the potential of using the electro-oxidation of GA for H_2 production remains unknown.

In summary, the use of electro-oxidation of biomass-based hydroxyacids such as LA and GA for electrolytic production of H_2 has been barely reported. Therefore, there are still many practical questions remaining in order to determine if this approach could become a potential technology for sustainable H_2 generation with simultaneous production of additional valuable chemicals. For

instance, the effect of the hydroxyacid structure on the reactivity and product selectivity is not well known. Several studies comparing the electrochemical reactivity of alcohol-based chemicals have been reported,[43,44] which has allowed understanding of many underlying factors in these reactions. However, this is still unexplored for organic hydroxyacids as well as how reaction conditions such as temperature or pH affect the overall reactivity. Fully understanding these electrochemical reactions will provide a roadmap to rationally select optimal conditions and reactants to achieve high-performance H_2 production by electrolysis of biomass-based hydroxyacids.

In this work, we studied two biomass-based hydroxyacids with different chemical structures in order to understand the role of the hydroxyacid structure on the electrochemical reactivity and thereby their potential to be used for sustainable H_2 production by electrolysis. These hydroxyacids were: a) lactic acid (LA), which only has one -OH group on the α carbon, and b) gluconic acid (GA), with multiple -OH groups across the chemical structure (Figure 2). A PdNi electrocatalyst prepared on a Ni foam substrate was used to enable the electro-oxidation of hydroxyacids at a relatively low potential, as previously demonstrated.[32] The role of several reaction parameters such as reactant concentrations, pH and temperature was studied to find the optimal conditions for the electro-oxidation reactions. Under these optimal conditions, the H_2 production rates and the anodic product distribution were measured to understand the differences between the two hydroxyacids, LA and GA, and their potential for the sustainable production of valuable chemicals.

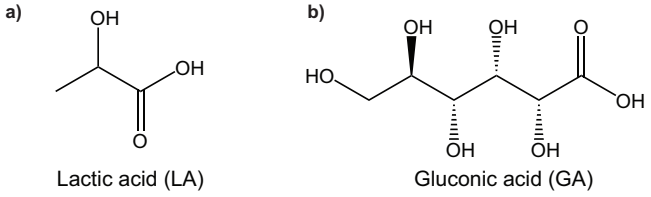

Figure 2. Chemical structures of organic hydroxyacids evaluated in this work: a) lactic acid (LA) and b) gluconic acid (GA).

EXPERIMENTAL

Solutions and reagents

Nickel(II) nitrate hexahydrate, palladium(II) chloride (> 59.0% Pd; >99.9%, metal basis), sodium chloride, sodium hydroxide, sulfuric acid (HPLC grade), pyruvic acid (≥ 98%), oxalic acid (≥ 99%) and acetic acid glacial (100%) were purchased from VWR (Radnor, PA, USA). Hydrochloric acid (37%), D-gluconic acid sodium salt (≥99%), D-glucaric acid potassium salt (≥ 98%), glycolic acid (99%), D-glucuronic acid sodium salt monohydrate (97.5 - 102.5%), L-glyceric acid sodium salt (≥ 95%), L-(+)-lactic acid (≥ 98%), glycolaldehyde dimer, 5-Keto-D-gluconic acid potassium salt (≥ 98%), potassium β-hydroxypyruvate (≥ 95%), D-(-)-arabinose (≥ 98%), glyoxylic acid monohydrate (≥ 98%), tartaric acid (≥ 98%) and succinic acid (≥ 98%) were purchased from Sigma-Aldrich (St. Louis, MO, USA). Tartronic acid (≥ 98%) was purchased from Alfa Aesar (Haverhill, MA, USA). Formic acid (98 – 100%) was purchased from Merck (Darmstadt, Germany). Nickel foam (1.6 mm thickness) was purchased from GoodFellow (Huntingdon, UK). All reagents were at least of analytical grade. Ultrapure water (18.2 MΩ cm) obtained with a Millipore DirectQ3 purification system from Merck Millipore (Burlington, MA, USA) was used throughout this work. Lactic and gluconic acid solutions were prepared daily with NaOH in ultrapure water. All experiments were carried out in alkaline pH since Ni (used as electrode substrate) is not stable in acidic conditions, especially at anodic potentials. Therefore, the concentration of NaOH was always equal or larger than the initial hydroxyacid concentration to ensure alkaline conditions, and accordingly, they were mostly in lactate or gluconate forms. For simplicity, they are named LA and GA hereafter.

Electrocatalyst preparation

PdNi catalysts were prepared onto Ni foam pieces (1.0 x 1.0 cm) by galvanostatic electrodeposition (-50 mA, 60 s) using a 25 mL two-electrode cell with a graphite rod as counter

electrode. A fresh solution of 100 mM $Ni(NO_3)_2$ and 2.5 mM $PdCl_2$ in 0.3 M HCl and 0.5 M NaCl was used for the electrodeposition. Under these conditions, the main component of palladium is the $[PdCl_4]^{2-}$ complex.[45] The solution was magnetically stirred at 300 rpm to ensure an efficient mass transport to the electrode. The Ni foam pieces were previously cleaned by ultrasonication in acetone (10 min) to remove adsorbed organic substances and in aqueous HCl solution (6 M) to remove oxide layers followed by thoroughly rinsing with ultrapure water. A small amount of epoxy was added to the Ni foam (Figure S1) to prevent the effect of solution capillarity and ensure a constant and defined contact area.[46] The prepared $PdNi/Ni_{foam}$ catalyst showed the typical surface processes of Pd catalysts in alkaline media as determined by cyclic voltammetry in 1 M NaOH (Figure S2). The electrochemical surface area (ECSA) was calculated for the $PdNi/Ni_{foam}$ catalyst: 143 ± 23 cm^2 (compared to the 2 cm^2 geometric area of the pristine Ni foam substrate). The ECSA was calculated using the charge under the peak of the PdO reduction process, assuming that the reduction of a monolayer of PdO requires 0.405 mC cm^{-2}, as widely reported previously.[47–49] The characterization of this catalyst by scanning electron microscopy (TEM), transmission electron microscopy (TEM) and Energy-dispersive X-ray spectroscopy (EDS) has been previously reported.[32] SEM images showed that the PdNi catalyst was formed by heterogeneous flower-shaped nanoparticles deposited on the 3D structure of the Ni foam with a coating thickness of about 1-2 μm. PdNi nanoparticles were formed by aggregates of smaller nanoparticles (from less than 10 nm to tens of nm) according to the TEM imaging. Diffraction and EDS data showed that the PdNi was formed by a polycrystalline Pd/NiO structure with an average Pd:Ni atomic ratio of 87:13.

Electrochemical measurements

Electrochemical measurements were conducted with a PAR273A potentiostat/galvanostat (Ametek) using a 100 mL three-electrode cell with $PdNi/Ni_{foam}$ as working electrode, a Pt mesh

counter electrode and a Hg/HgO reference electrode (1 M NaOH; RE-A6P, Bio-Logic) inserted into a Luggin capillary. The reference electrode was connected in parallel to a Pt wire in the same electrolyte with a 1 µF capacitor to ensure high-stability potential measurements. Temperature control was achieved by continuously flowing water from a thermostatic bath through a jacketed cell, and the solution was magnetically stirred at 300 rpm. Temperature effects on the reference electrode were not considered since the Luggin capillary allowed the physical separation of the electrode from the heated solution and the temperature effect was expected to be low (the thermal junction potential difference was also not considered). Current densities are presented normalized by the geometric area of the Ni foam substrate (2 cm^2). Dissolved oxygen was removed from the solution by bubbling nitrogen for at least 10 min before the experiments. Nitrogen was left open on the cell headspace during experiments to prevent oxygen re-entering the solution.

iR-corrected polarization curves were recorded using the current-interrupt technique. Briefly, the working electrode was polarized at the given current density and the current was interrupted. The decay of the potential was measured for 500 µs with a time resolution of 1 µs using a National Instrument cDAQ-9172 and NI-9223 device. Nonlinear parameter fitting was applied to calculate the *iR*-corrected potential value, $E(0)$, as previously discussed[50] using equation 1:

$$E(t) = E(0) - b \ln\left(1 + \frac{t\,j}{b\,C}\right) \quad \textbf{(1)}$$

where b is the Tafel slope, t is the time after the current interruption, j is the applied current density and C is the capacitance of the electrode.

Voltammetric onset potentials were calculated following a procedure previously reported.[51] Briefly, the voltammograms are represented as a derivative and the onset potential is taken as the potential where an extrapolated straight line from the derivative curve reached zero.

Product analysis experiments

Products generated at the anode and cathode after LA and GA electrolysis were analyzed. A 25 mL solution was employed for these experiments to achieve detectable concentrations in a short time, and the counter electrode was separated from the anodic compartment by a glass frit to avoid side reactions of the generated products (see Figure S3 for the cell schematics). The volume of H_2 produced at the cathode was measured using a gas displacement method. The cathodic compartment was filled with pure NaOH solution and connected by an empty tube to a graduated cylinder inverted and filled with water, which was displaced when H_2 was produced. Most of the cathodic compartment was kept outside the main cell to minimize water evaporation in the cathodic compartment during these experiments. The time required to produce a constant volume of H_2 (10 or 25 mL depending on the current density) was recorded in order to calculate the H_2 production rate at different current densities.

Product analysis of the oxidation reactions were carried out by High-Performance Liquid Chromatography (HPLC) on an Agilent 1260 Infinity II system with a refractive index detector (Agilent 1290 Infinity II RID) set on positive polarity. For LA reaction products, a sample volume of 10 µL was injected into an Agilent Hi-Plex H column (250 x 4.6 mm) using the autosampler of the instrument. 50 mM HPLC-grade H_2SO_4 was used as eluent at a flowing rate of 0.3 mL min^{-1}. For GA reaction products, a sample volume of 20 µL was injected into a double-column system containing a Bio-Rad Aminex HPX-87H (300 x 7.8 mm) and a Shodex SH1011 (300 x 8 mm). The mobile phase was 8 mm HPLC-grade H_2SO_4 flowing at a rate of 0.25 mL min^{-1}. The temperature of the columns and the detector was 30 °C in all cases.

Standards of pure reactants and possible products were used to evaluate retention times and calculate calibration curves in order to identify and quantify reactants and products. The volume of the solution was measured after the experiments in order to account for the evaporation during the reaction at high temperatures to calculate final concentrations accurately. To calculate the

product selectivity respect to a specific product, the number of moles (n) of the reactant consumed and product produced were obtained by HPLC. Then, the following equation 2 was used to calculate the selectivity for each product with a 1:1 stoichiometry with respect to the reactant:

$$Selectivity\ (\%) = 100 * \frac{n_{(product\ produced)}}{n_{(reactant\ consumed)}} \quad \textbf{(2)}$$

RESULTS AND DISCUSSION

Electrochemical oxidation of hydroxyacids: LA vs GA reactivity

In order to study the electrochemical oxidation of LA and GA, linear sweep voltammograms were recorded before and after the modification of the Ni foam substrate with the PdNi catalyst (Figure 3a). Significant peak-shaped anodic processes were observed for LA and GA oxidation only on the PdNi/Ni_{foam} catalyst under the studied potential range. Pd is required to enable the oxidation of both hydroxyacids at low potentials (onset potentials below -0.3 V vs Hg/HgO) and this would be beneficial in terms of energy requirements when exploiting these reactions for electrolytic production of H_2. This observation agrees well with previous reports where noble metal electrodes have shown better electrocatalytic properties than graphite, copper or nickel electrodes.[39,52] It is worth noting that Ni-based materials are known to electrocatalyze the oxidation of alcohols[15,53] and carbohydrates[54] in alkaline media through in situ generation of Ni (oxy)hydroxides[55] but the potential required for these reactions is considerably more positive than on Pd-based electrodes. The larger peak current recorded for the GA oxidation than for LA oxidation, at similar conditions (about ~4x larger at 1 M hydroxyacid in 1 M NaOH, Figure 3a), clearly shows the effect of the chemical structure on the electrochemical activity.

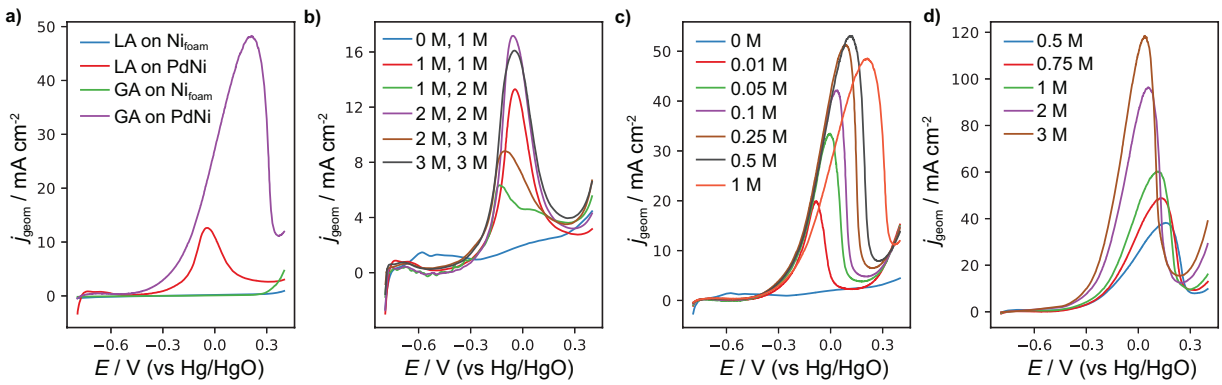

Figure 3. a) Linear sweep voltammograms (LSVs) for the oxidation of 1 M hydroxyacid in 1 M NaOH on pristine Ni foam and PdNi/Ni_{foam}. b) LSVs for LA oxidation at various concentrations of (LA, NaOH) on PdNi/Ni_{foam}. c) LSVs for GA oxidation at increasing concentrations of GA in 1 M NaOH on PdNi/Ni_{foam}. d) LSVs for 0.5 M GA oxidation at increasing concentrations of NaOH on PdNi/Ni_{foam}. Scan rate in all cases was 10 mV s^{-1}. Reaction temperature was 25 °C.

The concentrations of hydroxyacid and electrolyte (NaOH) significantly affected the electrochemical activity but to a greater extent for GA oxidation as shown in Figures 3b-d. The peak current densities only increased up to 2 M for LA oxidation (Figure 3b) and a higher pH was detrimental to the reaction according to the smaller peak current densities obtained for those cases. This experimental observation shows that OH^- ions are not strongly involved in the LA oxidation reaction under these conditions in agreement with the main product obtained in the reaction as determined by HPLC as discussed in more detail later. The smaller anodic current densities obtained when the concentration of NaOH was higher than that of LA also indicates that the LA oxidation is more effective at lower pH, which might be a result of a higher reactivity of the protonated form (lactic acid) than that of the de-protonated form (lactate). It is worth noting that conditions where the concentration of LA was higher than that of NaOH were not studied since the pH would be acidic and the Ni material would not be stable under oxidizing potentials. In contrast, GA oxidation was strongly affected by both the GA and NaOH concentrations, leading to larger peak current densities for increasing GA (Figure 3c) and NaOH (Figure 3d)

concentrations. This observation suggests that OH^- ions play an important role in the reactions taking place during the GA oxidation.

iR-corrected polarization curves for the same GA oxidation experiments were also recorded (Figure S4) in order to prevent any misleading interpretation due to possible distortions on the voltammetric profiles at high currents as a consequence of the *iR* drop. The *iR*-corrected polarization curves also reached higher current densities at higher GA and NaOH concentrations, following the same trend as the voltammetric response. Additional analysis of the *iR* polarization curves was carried out to obtain further knowledge about the GA electrocatalytic reaction by studying the relationship between the current densities at specific potentials and the corresponding GA and NaOH concentrations as described in the Supporting Information (Figure S5) and previously reported.[56,57] The order of reaction with respect to GA was smaller (0.58-0.64) than that of NaOH (0.62-1.39) in agreement with the strong influence of the NaOH concentration on the electrochemical reaction as clearly observed in the voltammetric and polarization curves. In addition, the order of reaction with respect to NaOH decreased with the overpotential but it was practically constant for GA, which also shows that the influence of the NaOH concentration on the reaction rate is larger at the onset of the reaction. This observation is likely a consequence of different electrochemical reactions taking place at different potentials.

The role of temperature on LA and GA electrochemical oxidation

The role of the temperature on the LA and GA oxidation reactions was studied by recording a series of voltammograms at increasing temperatures (25-80 °C). Increasing the temperature led to higher current densities for both reactions as shown in Figures 4a-b, demonstrating that the reaction temperature is an important parameter to enhance the oxidation rate and, consequently, the H_2 production in the cathode. Anodic peak currents increased from 11 ± 2 mA cm^{-2} to 159 ± 11 mA cm^{-2} (more than 14 times) for LA oxidation after increasing the temperature from 25 to 80 °C. For GA oxidation, the increment was from 109 ± 6 mA cm^{-2} at 25 °C to more than 650 mA

cm^{-2} at 80 °C, reaching the potentiostat current limit (~1.3 A). This observation is strong proof of the high activity of the $PdNi/Ni_{foam}$ catalyst for the GA oxidation reaction even if these temperatures can be considered relatively mild (boiling point of GA is 417 °C) and shows that this system is very promising for high-performance H_2 production by electrolysis. The onset potentials also decreased with increasing temperatures for both reactions (Figures S6 and S7): from -0.17 ± 0.01 V at 25 °C to -0.40 ± 0.03 V at 80 °C for LA oxidation, and from -0.36 ± 0.02 V at 25 °C to -0.51 ± 0.02 V at 80 °C for GA oxidation. It is worth noting that the bare Ni foam was also not active at high temperatures (Figure S8) in this potential range.

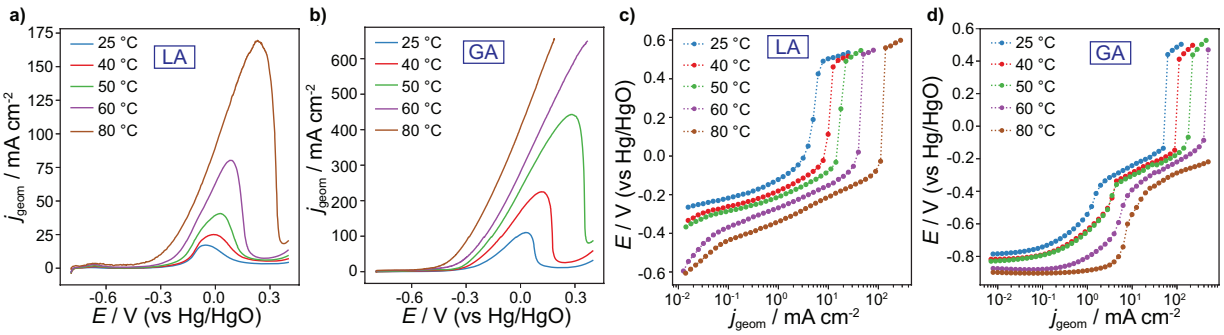

Figure 4. LSVs for the oxidation of **a)** 2 M LA in 2 M NaOH and **b)** 0.5 M GA in 3 M NaOH at increasing reaction temperatures on $PdNi/Ni_{foam}$. Scan rate was 10 mV s^{-1}. *iR* corrected polarization curves for the oxidation of **c)** 2 M LA in 2 M NaOH and **d)** 0.5 M GA in 3 M NaOH at increasing reaction temperatures on $PdNi/Ni_{foam}$.

iR-corrected polarization curves were also recorded to study the role of temperature on the LA and GA oxidation reactions avoiding any effect of the *iR* drop, which might be considerable under the high currents recorded (reaching >1 A, as discussed). These experiments also allow the calculation of kinetic parameters such as slopes of the log *j* vs *E* representation or activation energies more accurately than using voltammetric data (again, due to the *iR* drop). Figures 4c-d show the *iR*-corrected polarization curves at increasing temperatures for LA and GA oxidation reactions, respectively. Similar to the voltammetric response, the reactions also occurred at lower potentials and higher current densities with increasing temperatures. In order to compare the effect of the temperature on the LA and GA oxidation reactions, the relative enhancement defined as the

current density at a specific temperature divided by the current density at 25 °C is shown in Figure S9. This representation shows that the electrochemical reactivity of LA was enhanced at a greater extent than that of the GA by increasing the reaction temperature.

Further analysis of the polarization curves at different temperatures was carried out by fitting the currents for the hydroxyacids oxidation to a linear equation of the form $E = a + b \log_{10}(j)$, which also provides mechanistic and kinetic information. Figure S10a reveals that the LA oxidation reaction likely has two different rate determining steps at low and high overpotentials, respectively, when the reaction temperature is low (25-50 °C) since two linear regions with different slopes are found (about 60-70 mV dec^{-1} and 115-135 mV dec^{-1}). However, only one linear region (106-116 mV dec^{-1}) was found at the highest temperatures (60-80 °C), suggesting that the same rate determining step dominates over the whole potential range. The slopes of the polarization curves for the GA oxidation (Figure S10b) were more homogeneous throughout the full range of temperatures evaluated (138-147 mV dec^{-1}) indicating that the rate limiting step of the GA oxidation reaction is the same at different temperatures and overpotentials.

The estimation of the apparent energy of activation (E_a) can provide further important information about the reaction kinetics of the LA and GA oxidation reactions. E_a can be calculated using the Arrhenius equation adapted to electrochemical reactions[58] (equation 3) since the current density is a factor of the rate constant of the reaction:

$$j = A\, e^{\frac{-E_a}{RT}} \quad \textbf{(3)}$$

where j is the current density, A is the pre-exponential factor, T is the temperature and R is the ideal gas constant. Arrhenius plots can be obtained by plotting the $\ln j$ as a function of T^{-1} at different potentials as the reaction rate (i.e. j) depends on the applied overpotential (according to Butler-Volmer kinetics).[59] For instance, Figures 5a-b show the Arrhenius plots obtained at different potentials for LA and GA oxidation reactions, while Figures 5c-d show the dependence

between the E_a and the applied potential. Clearly opposing behavior was found for the LA and GA oxidation reactions. The E_a decreased with increasingly positive potentials for LA oxidation up to -0.15 V (vs Hg/HgO) approximately, which is the expected behavior as the reaction rate typically increases with the overpotential. At high enough potentials, the apparent E_a value becomes constant with increasing potentials, meaning that the reaction kinetics do not increase further. Several factors can be responsible for such an observation as e.g. the mass transport rate could become a limiting factor of the reaction at high overpotentials or the effect produced by the simultaneous oxidation of Pd active sites at those high potentials forming inactive Pd oxides,[13,60] which would result in an apparent decrease of the LA oxidation kinetics. In contrast, E_a increased with the overpotential for GA oxidation. Whilst this behavior seems counterintuitive according to Butler-Volmer kinetics, the complexity of the reactions taking place during the GA oxidation (see product analysis below) may lead to unexpected empirical observations. This behavior has been previously observed for ethanol oxidation on different electrocatalysts[53,61,62] and was associated with adsorption of ethanol to the electrode surface as the rate determining step and also for carbohydrates oxidation on gold electrodes,[63] although in the latter case a volcano-shaped curve was obtained (i.e. initial increment of E_a with the overpotential up to an inversion point where the E_a starts decreasing with overpotential). It is worth noting that the complexity of the LA and GA oxidation reactions makes the interpretation of these values quite difficult and any quantitative conclusions are not definitive. From a comparative point of view, the E_a values obtained for GA oxidation (38-50 kJ mol^{-1}) are smaller than those obtained for LA oxidation (55-77 kJ mol^{-1}) in agreement with the much higher electrochemical activity and lower onset potentials found for GA oxidation. There is a lack of reported data for E_a values from electrochemical oxidation of LA or GA as a consequence of the few studies published, so a direct comparison with other electrocatalysts cannot be carried out. In any case, it might be interesting to compare data with previous reports of homo/heterogeneous catalysis for LA or GA oxidations. The values of E_a obtained from our study are in the same order of magnitude as those reported from

hetero/homogeneous catalysis for LA oxidation. For instance, 45 kJ mol^{-1} was calculated for lactic acid oxidation to pyruvic acid by chromic acid in presence of Ce(IV).[64] In the case of oxidation of ethyl lactate to ethyl pyruvate, 59.7 kJ mol^{-1} and 103.4 kJ mol^{-1} were obtained using catalysts based on MoVNbO[65] and a titanium-based zeolite,[66] respectively. E_a values for GA oxidation to a range of different products (with ~50% tartaric acid selectivity) were also in the same order with 46.5 and 90.2 kJ mol^{-1} reported for Pt/TiO_2 and AuPt/TiO_2 heterogeneous catalysts,[40] respectively.

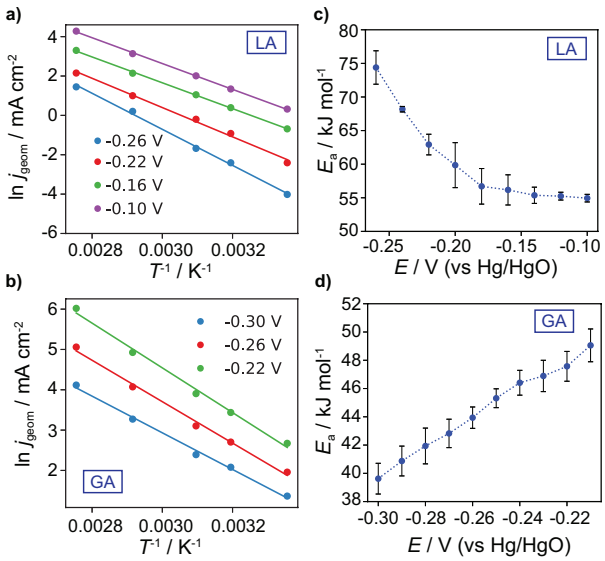

Figure 5. Representative Arrhenius plots at different potentials for the oxidation of a) 2 M LA in 2 M NaOH and b) 0.5 M GA in 3 M NaOH. Dependence between the apparent activation energy (E_a) and the potential for c) LA oxidation and d) GA oxidation. Data obtained from the *iR*-corrected polarization curves as shown in Figures 4c-d. Standard deviations are calculated from n=3 experiments.

Time-dependent performance of LA and GA electrochemical oxidation

The time-dependent performance of LA and GA oxidation reactions on the PdNi/Ni_{foam} catalyst was studied by recording *iR*-corrected galvanostatic curves at different current densities (Figure 6). In all cases, the galvanostatic response showed an initial shift of the potential until reaching a quasi-constant value, which was higher at higher applied current densities as expected. Quasi-constant potential values between -0.35 and -0.15 V vs Hg/HgO were recorded for LA oxidation

at current densities between 10-50 mA cm^{-2}, which demonstrated that LA oxidation takes place at relatively low potentials and acceptable conversion rates (i.e. current densities) under these conditions. At 100 mA cm^{-2} (brown curve in Figure 6a), the catalyst became deactivated before reaching the end of the experiment as shown by the sharp potential shift to values where water oxidation is able to support that current density (+0.6 V vs Hg/HgO). Interestingly, the initial catalyst response can be recovered by regenerating the catalyst surface after applying a negative potential (-0.8 V vs Hg/HgO) for a short time (5 s) as shown in the black curve of Figure 6a. Catalyst deactivation likely occurs by the formation of an oxide layer on Pd,[60] which is promoted at high potentials and makes the Pd sites inactive for alcohol oxidation. This Pd oxide layer can be removed by electrochemical reduction inducing the regeneration of the catalyst surface (Pd active sites) recovering the initial response for LA oxidation. This surface reactivation process has been previously exploited to increase the reaction rate and stability of Pd-based catalysts for LA oxidation[32] and other reactions.[67] Galvanostatic curves were recorded at higher current densities (75-200 mA cm^{-2}) to study the time-dependent GA oxidation which also took place at very low potentials (Figure 6b) and significantly lower than those obtained for the LA oxidation. For instance, the quasi-constant potential value for LA oxidation at 50 mA cm^{-2} was about -0.18 V while that for GA oxidation at 75 mA cm^{-2} was -0.32 V. In this context, it was possible to carry out GA oxidation at very high current densities (400 mA cm^{-2}) still at very low potentials (less than -0.15 V) and with only a small increase of 60 mV since the beginning of the experiment after 3 hours of electrolysis (Figure 6c). Achieving the GA oxidation at these high rates (i.e. high current densities) and low potentials has a two-fold positive effect. On one hand, this high reaction rate means that H_2 production can be performed at an industrially-relevant production rate (for instance, the theoretical value at 100% faradaic efficiency at 400 mA cm^{-2} is ~5.6 mL min^{-1}). On the other hand, the Pd oxidation resulting in the catalyst deactivation is slow at these low potentials and, therefore, the catalyst is very stable for GA oxidation as demonstrated by the absence of a shift to higher positive potentials as was observed for LA oxidation.

It is worth emphasizing the advantage in energy requirements when replacing the anodic reaction of water oxidation by hydroxyacids oxidation. Figure 6d shows *iR*-corrected galvanostatic curves for water oxidation under similar conditions to that of LA and GA oxidation. The hydroxyacids oxidation took place at a significantly lower potential than water oxidation, with potential differences of 0.797 and 0.991 V (at 200 s) for LA at 50 mA cm^{-2} and GA at 100 mA cm^{-2}, respectively. This strong decrease in the potential of the anodic reaction due to the introduction of hydroxyacids oxidation can lead to significant savings in energy requirements for H_2 production. Which, under those conditions were 21.2 and 26.3 kWh kg^{-1} H_2 less for LA and GA oxidation, respectively, than for water oxidation (see calculations in section 2 of Supporting Information).

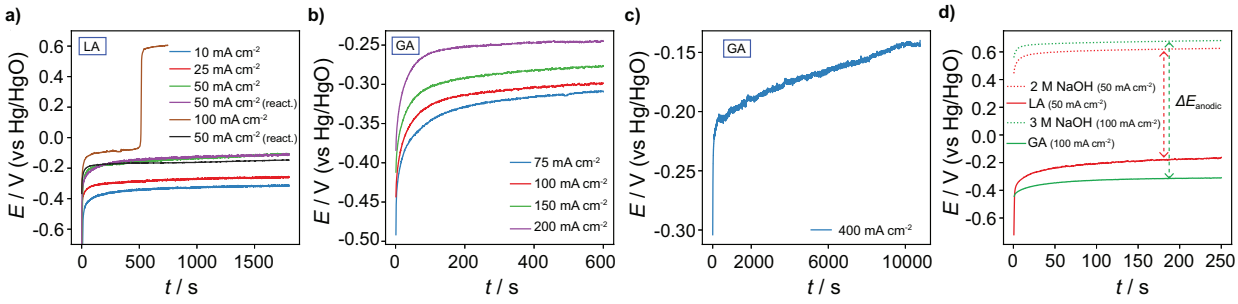

Figure 6. a) *iR*-corrected galvanostatic response for the oxidation of 2 M LA in 2 M NaOH at different current densities (10-100 mA cm^{-2}). Abbreviations: "rep." means a repeated experiment at 50 mA cm^{-2} and "react." means a repeated experiment at 50 mA cm^{-2} after the catalyst reactivation by applying -0.8 V for 5 s. **b)** *iR*-corrected galvanostatic response for the oxidation of 0.5 M GA in 3 M NaOH at different current densities (75-200 mA cm-2). **c)** Long-term (3h) *iR*-corrected galvanostatic response for the oxidation of 0.5 M GA in 3 M NaOH at 400 mA cm^{-2}. **d)** *iR*-corrected galvanostatic curves for the oxidation of 2 M LA in 2 M NaOH at 50 mA cm^{-2}, 0.5 M GA in 3 M NaOH at 100 mA cm^{-2}, and water oxidation at 50 mA cm^{-2} (2 M NaOH) and 100 mA cm^{-2} (3 M NaOH). ΔE_{anodic} illustrates the difference in the anodic potential between the oxidation of hydroxyacids and water oxidation. Reaction temperature was 80 °C in all cases.

Product analysis for LA and GA electrochemical oxidations

The products generated from the LA and GA oxidations were measured in both the anodic and cathodic compartments as follows: the H_2 produced at the cathode was measured online by a gas displacement method and the product distribution for the anodic reaction was analyzed offline by HPLC. Figures 7a-b show the H_2 production rate in mL min^{-1} at different applied current densities (galvanostatic experiments) together with the theoretical value calculated by Faraday's law of electrolysis. Faradaic efficiencies were close to 100% for the H_2 production in all cases, as expected using a divided cell where the cathodic compartment is filled with a pure NaOH solution and only the water reduction reaction occurs on the Pt counter electrode. More interesting was the product analysis carried out after the LA and GA oxidation reactions took place at the anodic compartment. Figure 7c shows the product distribution calculated for the LA oxidation, which shows a good selectivity to pyruvate production (64 ± 4 %). This reaction would entail the transfer of two electrons according to the chemical equation shown in Figure 8, while the OH^- ions are only involved to neutralize the protons resulting from the reaction. The remaining products can be attributed to two HPLC signals observed at short retention times (Figure S11) that also increased with the reaction time. Further oxidation of LA might lead to acetaldehyde or acetate as reported previously,[27,29,31] but these products were not detected in the HPLC chromatograms as they would appear at longer retention times. Therefore, the unknown species obtained during this reaction are expected to be some kind of oligomerization products, as they can be formed under certain conditions.[68,69] The product distribution was significantly more complex for the GA oxidation as shown in Figure 7d (product distribution) and Figure S12 (HPLC chromatogram). Several products such as tartronate (20.9% selectivity), hydroxypyruvate (15.6%), oxalate (14.7%), formate (12.0%), lactate (9.9%), glycolate (5.1%), glucarate (3.5%), glycerate (1.6%) and acetate (0.9%) were identified from the HPLC analysis. Mesoxalate was also detected but at a very small amount that did not allow to carry out its quantification precisely. All the detected

products add for 84.3% of the consumed GA (79.7% conversion in 2 h). The rest of the reaction products (14.7%) can be ascribed to a few unassigned HPLC peaks, and it is reasonable to assume that some CO_2 (carbonate) can also be formed by oxidation of formate or other reaction intermediates. Formate was identified as one of the GA oxidation products and its oxidation to CO_2 has been widely reported with Pd-based electrocatalysts.[70,71] The GA oxidation certainly follows a more complex reaction mechanism than the LA oxidation and proposed pathways for the detected products are represented in Figure 9 based on previous reports in the literature from the oxidation of similar species such as GA, glucose or glycerol.[40,72–74] Briefly, we propose that the GA oxidation takes place preferentially through the oxidation of the carbons furthest from the carboxylic group (C_6 and C_5). This is in agreement with the lower reactivity found for LA oxidation where the oxidizable C-OH group is in C_2, near the carboxylic group, which may ~~to~~ provide a stabilizing effect for the C-OH oxidation according to the higher onset potentials observed for the LA oxidation reaction. Thus, the oxidation of C_6 would produce glucarate through initial formation of glucuronate by a direct oxidative mechanism where the C-C bonds remain intact. The oxidation of C_5 would lead to the formation of 5-ketogluconate, which can suffer C-C cleavage by a retro-aldol reaction to form a mixture of several products by a cascade of electrochemical and chemical reactions as shown in Figure 9, which would explain the formation of all the detected products. Glucuronate can also rapidly isomerize to 5-ketogluconate[74] and that might also be an alternative generation in case the oxidation of C_6 takes place more favorably than the oxidation of C_5. It is worth noting that both glucuronate and 5-ketogluconate were not detected by HPLC, which suggests that both the formation of glucarate and the retro-aldol C-C cleavage of 5-ketogluconate are very rapid reactions. There are several possible pathways through C-C cleavage that would explain the formation of all the detected products, but the pathway proposed here also agrees well with the high amount of tartronate and oxalate detected by HPLC (35.6% of all products) as these products can be formed by several reactions through the proposed pathway. The small amount found for mesoxalate indicates that

either the oxidation of tartronate to mesoxalate does not occur easily or the mesoxalate is quite reactive and quickly forms oxalate and carbonate. In addition, only a small amount of acetate was detected proving that the oxidative C-C cleavage of LA does not occur easily in agreement with the experiments involving the direct oxidation of LA, where no acetate was found. Interestingly, pyruvate was not detected by HPLC during the GA oxidation even if LA was found at an amount greater than that of molecules denser with OH- groups such as glycerate and glucarate. This is indicative of strong competition for active sites between the initial GA, other reactive species mentioned and LA, and can explain the lack of pyruvate formation, as the oxidation of GA or other highly reactive products seems to take place more preferentially than the LA oxidation.

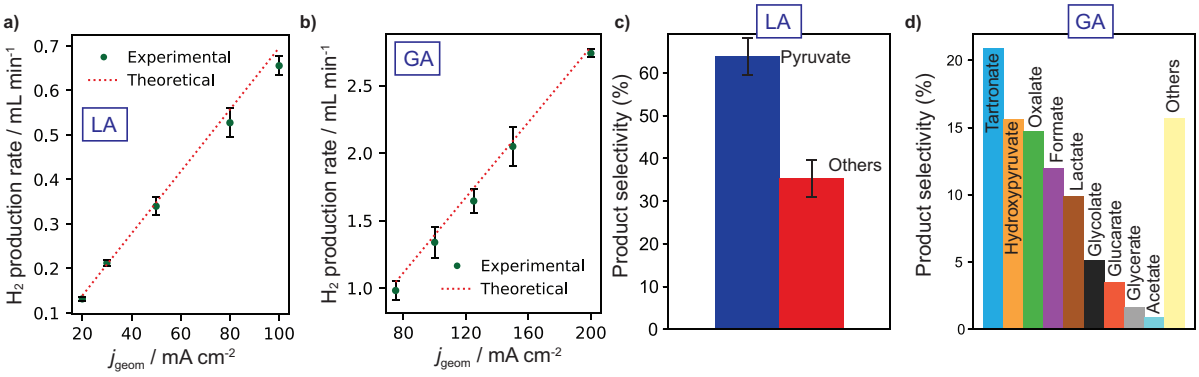

Figure 7. H_2 production rate in mL min^{-1} recorded during the oxidation of **a)** 2 M LA in 2 M NaOH and **b)** 0.5 M GA in 3 M NaOH at different applied current densities. Blue dots are experimental measurements and the red line is the theoretical value expected for 100% Faradaic efficiency. The cathodic compartment was filled with NaOH solution. Standard deviations are calculated from n=3 experiments. **c)** Product distribution obtained by HPLC analysis after the oxidation of 1 M LA in 1 M NaOH by applying a current density of 25 mA cm^{-2} for 2 h. **d)** Product distribution obtained by HPLC analysis after the oxidation of 0.25 M GA in 3 M NaOH by applying 200 mA cm^{-2} for 2 h. Reaction temperature was 80 °C in all cases.

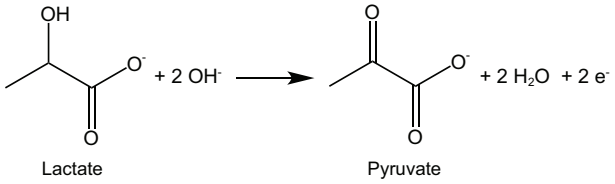

Figure 8. Reaction scheme for the oxidation of LA to pyruvate.

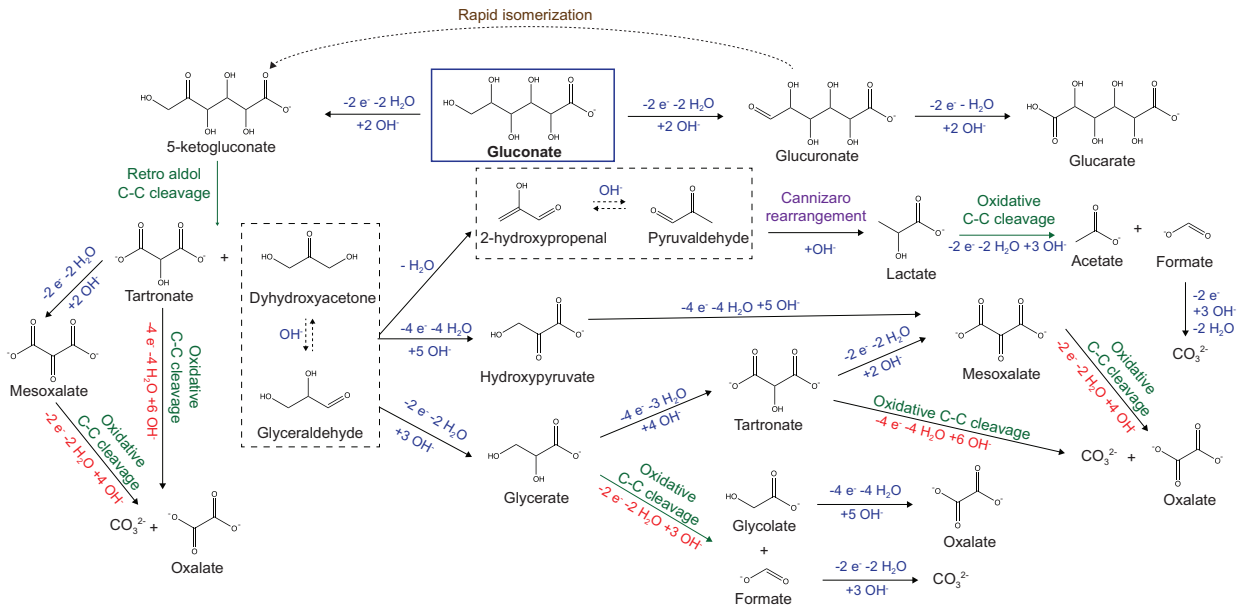

Figure 9. Proposed reaction pathways for GA oxidation.

In a comparative context, it seems clear that the structure of the hydroxyacid plays a significant role in several aspects of the electro-oxidation reaction. For instance, a lower electrochemical activity was found for LA oxidation, which only has one -OH group in the α position, demonstrating that this kind of structure is less reactive compared to hydroxyacids with a larger density of -OH groups along the molecule such as in the case of GA. The higher electrochemical activity observed for GA oxidation (i.e. larger current densities) might also be a consequence of the larger number of transferred electrons needed during the cascade of oxidation reactions required to generate all detected products. This complex pathway would be possible through facile C-C bond breaking when contiguous C-OH groups are present in the chemical structure. Therefore, from a point of view towards H_2 production, a more reactive hydroxyacid leading to high current densities such as GA is beneficial in order to achieve a high H_2 production rate. In contrast, the low product selectivity found for GA oxidation makes it more challenging to exploit the generated products in other value-added applications as in a biorefinery context, because complex separation steps might be required. The biorefinery route could be more appropriate for

more selective reactions such as LA oxidation where a main product (pyruvate) is obtained, which makes the separation steps easier to collect the pure product for subsequent applications, and the advantage in energy requirements for H_2 production compared to water oxidation is still significant.

CONCLUSIONS

In conclusion, this work shows that the electrochemical oxidation of organic hydroxyacids such as LA and GA, is a promising approach for the sustainable generation of clean H_2 by electrolysis with significant improvements in energy requirements compared to water oxidation (more than 20 kWh kg^{-1} H_2). Both hydroxyacids were easily oxidized on the $PdNi/Ni_{foam}$ electrocatalyst at low potentials, but the GA oxidation achieved higher industrially-relevant current densities and, thus, higher H_2 production rates than the LA oxidation. In contrast, LA oxidation was a more selective reaction leading to the production of mainly pyruvate. This work highlights the importance of the chemical structure of organic hydroxyacids on the activity and selectivity of electro-oxidation reactions and provides a roadmap to select appropriate organic hydroxyacids depending on whether the main goal is H_2 generation or selective production of value-added chemicals for further applications. It is worth noting that experimental conditions such as catalyst structure, mass transfer rate, temperature, pH and applied potential can not only affect the reactivity, as evaluated in this work, but also the product selectivity.[16,75,76] Therefore, exploring conditions where the reaction selectivity can be enhanced towards specific highly-valuable chemicals while keeping a good H_2 generation rate would be a very interesting subsequent study in addition to the evaluation of further biomass-based organic hydroxyacids.

ACKNOWLEDGEMENTS

This work was supported by the Swedish Foundation for Strategic Research (SSF), through grant number EM16-0010 and by the Swedish Energy Agency (Project 44666-1).

REFERENCES

[1] S. Chu, A. Majumdar, *Nature* **2012**, *488*, 294–303.
[2] V. Vogl, M. Åhman, L. J. Nilsson, *J. Clean. Prod.* **2018**, *203*, 736–745.
[3] P. H. Pfromm, *J. Renew. Sustain. Energy* **2017**, *9*, 034702.
[4] M. G. Walter, E. L. Warren, J. R. McKone, S. W. Boettcher, Q. Mi, E. A. Santori, N. S. Lewis, *Chem. Rev.* **2010**, *110*, 6446–6473.
[5] A. Buttler, H. Spliethoff, *Renew. Sustain. Energy Rev.* **2018**, *82*, 2440–2454.
[6] B. You, X. Liu, N. Jiang, Y. Sun, *J. Am. Chem. Soc.* **2016**, *138*, 13639–13646.
[7] H. A. Miller, A. Lavacchi, F. Vizza, *Curr. Opin. Electrochem.* **2020**, *21*, 140–145.
[8] Y. X. Chen, A. Lavacchi, H. A. Miller, M. Bevilacqua, J. Filippi, M. Innocenti, A. Marchionni, W. Oberhauser, L. Wang, F. Vizza, *Nat. Commun.* **2014**, *5*, 4036.
[9] M. Simões, S. Baranton, C. Coutanceau, *ChemSusChem* **2012**, *5*, 2106–2124.
[10] K. Kohli, R. Prajapati, B. Sharma, *Energies* **2019**, *12*, 233.
[11] A. Corma, S. Iborra, A. Velty, *Chem. Rev.* **2007**, *107*, 2411–2502.
[12] M. Besson, P. Gallezot, C. Pinel, *Chem. Rev.* **2014**, *114*, 1827–1870.
[13] R. B. Araujo, D. Martín-Yerga, E. C. dos Santos, A. Cornell, L. G. M. Pettersson, *Electrochimica Acta* **2020**, *360*, 136954.
[14] C. H. W. Kelly, T. M. Benedetti, A. Alinezhad, J. J. Gooding, R. D. Tilley, *ChemCatChem* **2019**, cctc.201901263.
[15] D. Martín-Yerga, G. Henriksson, A. Cornell, *Electrocatalysis* **2019**, *10*, 489–498.
[16] D. Martín-Yerga, G. Henriksson, A. Cornell, *Int. J. Hydrog. Energy* **2021**, *46*, 1615–1626.
[17] M. S. E. Houache, K. Hughes, A. Ahmed, R. Safari, H. Liu, G. A. Botton, E. A. Baranova, *ACS Sustain. Chem. Eng.* **2019**, *7*, 14425–14434.
[18] A. Van Heiningen, *Pulp Pap Can.* **2006**, *107*, 38–43.
[19] L. Reyes, C. Nikitine, L. Vilcocq, P. Fongarland, *Green Chem.* **2020**, *22*, 8097–8115.
[20] P. Mäki-Arvela, I. L. Simakova, T. Salmi, D. Yu. Murzin, *Chem. Rev.* **2014**, *114*, 1909–1971.
[21] J. J. Bozell, G. R. Petersen, *Green Chem.* **2010**, *12*, 539.
[22] M. Dusselier, P. Van Wouwe, A. Dewaele, E. Makshina, B. F. Sels, *Energy Environ. Sci.* **2013**, *6*, 1415.
[23] Y. Fan, C. Zhou, X. Zhu, *Catal. Rev.* **2009**, *51*, 293–324.
[24] C. Zhang, T. Wang, Y. Ding, *Appl. Catal. Gen.* **2017**, *533*, 59–65.
[25] N. Maleki, M. Eiteman, *Fermentation* **2017**, *3*, 8.
[26] P. Xu, J. Qiu, C. Gao, C. Ma, *J. Biosci. Bioeng.* **2008**, *105*, 169–175.
[27] G. Horányi, *J. Electroanal. Chem. Interfacial Electrochem.* **1981**, *117*, 131–137.
[28] G. C. Sedenho, P. T. Lee, H. S. Toh, C. Salter, C. Johnston, N. R. Stradiotto, R. G. Compton, *Int J Electrochem Sci* **2016**, *11*, 11.
[29] A. Yuksel, M. Sasaki, M. Goto, *Ind. Eng. Chem. Res.* **2011**, *50*, 728–734.
[30] C. Chen, A. J. Bloomfield, S. W. Sheehan, *Ind. Eng. Chem. Res.* **2017**, *56*, 3560–3567.
[31] Z. Xixi, P. Qian, B. Wang, *Appl. Microbiol. Biotechnol.* **2019**, *103*, 4045–4052.
[32] D. Martín-Yerga, X. Yu, I. Terekhina, G. Henriksson, A. Cornell, *Chem. Commun.* **2020**, *56*, 4011–4014.
[33] A. M. Cañete-Rodríguez, I. M. Santos-Dueñas, J. E. Jiménez-Hornero, A. Ehrenreich, W. Liebl, I. García-García, *Process Biochem.* **2016**, *51*, 1891–1903.
[34] O. V. Singh, R. Kumar, *Appl. Microbiol. Biotechnol.* **2007**, *75*, 713–722.
[35] C. Liu, J. Zhang, J. Huang, C. Zhang, F. Hong, Y. Zhou, G. Li, M. Haruta, *ChemSusChem* **2017**, *10*, 1976–1980.
[36] H. Zhang, N. Li, X. Pan, S. Wu, J. Xie, *Green Chem.* **2016**, *18*, 2308–2312.
[37] P. N. Amaniampong, K. Li, X. Jia, B. Wang, A. Borgna, Y. Yang, *ChemCatChem* **2014**, *6*, 2105–2114.
[38] X. Tan, W. Deng, M. Liu, Q. Zhang, Y. Wang, *Chem. Commun.* **2009**, 7179.
[39] G. Moggia, T. Kenis, N. Daems, T. Breugelmans, *ChemElectroChem* **2020**, *7*, 86–95.
[40] M. Liu, X. Jin, G. Zhang, Q. Xia, L. Lai, J. Wang, W. Zhang, Y. Sun, J. Ding, H. Yan, C. Yang, *ACS Catal.* **2020**, *10*, 10932–10945.
[41] G. Pezzatini, H. Wei, R. Guidelli, F. Pergola, *Electroanalysis* **1992**, *4*, 129–132.
[42] C.-F. Chou, T.-C. Chou, *J. Appl. Electrochem.* **2003**, *33*, 741–745.
[43] Y. Kwon, S. C. S. Lai, P. Rodriguez, M. T. M. Koper, *J. Am. Chem. Soc.* **2011**, *133*, 6914–6917.

[44] A. Santasalo-Aarnio, Y. Kwon, E. Ahlberg, K. Kontturi, T. Kallio, M. T. M. Koper, *Electrochem. Commun.* **2011**, *13*, 466–469.
[45] J. M. van Middlesworth, S. A. Wood, *Geochim. Cosmochim. Acta* **1999**, *63*, 1751–1765.
[46] W. Zheng, M. Liu, L. Y. S. Lee, *ACS Energy Lett.* **2020**, *5*, 3260–3264.
[47] S. Trasatti, O. A. Petrii, *J. Electroanal. Chem.* **1992**, *327*, 353–376.
[48] M. Łukaszewski, M. Soszko, A. Czerwinski, *Int. J. Electrochem. Sci.* **2016**, *11*, 4442–4469.
[49] T. Chierchie, C. Mayer, W. J. Lorenz, *J. Electroanal. Chem. Interfacial Electrochem.* **1982**, *135*, 211–220.
[50] B. Endrődi, S. Sandin, V. Smulders, N. Simic, M. Wildlock, G. Mul, B. T. Mei, A. Cornell, *J. Clean. Prod.* **2018**, *182*, 529–537.
[51] B. D. Ferreira, L. M. Alencar, G. C. da Silva, G. Maia, C. A. Martins, *Electrocatalysis* **2018**, *9*, 314–322.
[52] L. J. Torres-Pacheco, L. Álvarez-Contreras, V. Lair, M. Cassir, J. Ledesma-García, M. Guerra-Balcázar, N. Arjona, *Fuel* **2019**, *250*, 103–116.
[53] A. F. B. Barbosa, V. L. Oliveira, J. van Drunen, G. Tremiliosi-Filho, *J. Electroanal. Chem.* **2015**, *746*, 31–38.
[54] B. Pérez-Fernández, D. Martín-Yerga, A. Costa-García, *RSC Adv.* **2016**, *6*, 83748–83757.
[55] D. Chen, S. D. Minteer, *J. Power Sources* **2015**, *284*, 27–37.
[56] R. Jiang, D. T. Tran, J. P. McClure, D. Chu, *ACS Catal.* **2014**, *4*, 2577–2586.
[57] D. Chu, S. Gilman, *J. Electrochem. Soc.* **1996**, *143*, 1685–1690.
[58] Z.-D. He, Y.-X. Chen, E. Santos, W. Schmickler, *Angew. Chem. Int. Ed.* **2018**, *57*, 7948–7956.
[59] E. J. F. Dickinson, A. J. Wain, *J. Electroanal. Chem.* **2020**, *872*, 114145.
[60] L. Wang, A. Lavacchi, M. Bellini, F. D'Acapito, F. D. Benedetto, M. Innocenti, H. A. Miller, G. Montegrossi, C. Zafferoni, F. Vizza, *Electrochimica Acta* **2015**, *177*, 100–106.
[61] F. Colmati, E. Antolini, E. R. Gonzalez, *J. Power Sources* **2006**, *157*, 98–103.
[62] L. S. R. Silva, I. G. Melo, C. T. Meneses, F. E. Lopez-Suarez, K. I. B. Eguiluz, G. R. Salazar-Banda, *J. Electroanal. Chem.* **2020**, *857*, 113754.
[63] Y. Holade, A. B. Engel, K. Servat, T. W. Napporn, C. Morais, S. Tingry, D. Cornu, K. B. Kokoh, *J. Electrochem. Soc.* **2018**, *165*, H425–H436.
[64] M. Ahmadmalik, Z. Khan, *Acta Phys.-Chim. Sin.* **2007**, *23*, 1013–1017.
[65] L. Zhang, R. Wang, L. Song, X. Zhao, Q. Fan, H. Li, Q. Yu, X. Li, J. Zeng, C. Zhang, T. Liu, Z. Wang, *Catal. Lett.* **2019**, *149*, 840–850.
[66] T. Lu, J. Zou, Y. Zhan, X. Yang, Y. Wen, X. Wang, L. Zhou, J. Xu, *ACS Catal.* **2018**, *8*, 1287–1296.
[67] J. Gopeesingh, M. A. Ardagh, M. Shetty, S. T. Burke, P. J. Dauenhauer, O. A. Abdelrahman, *ACS Catal.* **2020**, *10*, 9932–9942.
[68] M. I. Guzmán, A. J. Colussi, M. R. Hoffmann, *J. Phys. Chem. A* **2006**, *110*, 3619–3626.
[69] A. E. Reed Harris, B. Ervens, R. K. Shoemaker, J. A. Kroll, R. J. Rapf, E. C. Griffith, A. Monod, V. Vaida, *J. Phys. Chem. A* **2014**, *118*, 8505–8516.
[70] F. J. Vidal-Iglesias, R. M. Arán-Ais, J. Solla-Gullón, E. Garnier, E. Herrero, A. Aldaz, J. M. Feliu, *Phys. Chem. Chem. Phys.* **2012**, *14*, 10258.
[71] X. Liu, Y. Bu, T. Cheng, W. Gao, Q. Jiang, *Electrochimica Acta* **2019**, *324*, 134816.
[72] C. Dai, L. Sun, H. Liao, B. Khezri, R. D. Webster, A. C. Fisher, Z. J. Xu, *J. Catal.* **2017**, *356*, 14–21.
[73] E. Derrien, M. Mounguengui-Diallo, N. Perret, P. Marion, C. Pinel, M. Besson, *Ind. Eng. Chem. Res.* **2017**, *56*, 13175–13189.
[74] X. Jin, M. Zhao, M. Vora, J. Shen, C. Zeng, W. Yan, P. S. Thapa, B. Subramaniam, R. V. Chaudhari, *Ind. Eng. Chem. Res.* **2016**, *55*, 2932–2945.
[75] M. B. C. de Souza, R. A. Vicente, V. Y. Yukuhiro, C. T. G. V. M. T. Pires, W. Cheuquepán, J. L. Bott-Neto, J. Solla-Gullón, P. S. Fernández, *ACS Catal.* **2019**, *9*, 5104–5110.
[76] C. Zhu, B. Lan, R.-L. Wei, C.-N. Wang, Y.-Y. Yang, *ACS Catal.* **2019**, *9*, 4046–4053.

TABLE OF CONTENTS

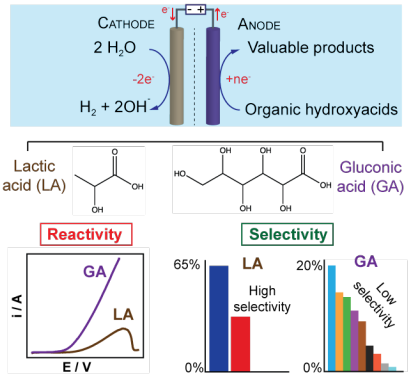

Two-edge sword: Hydroxyacids electro-oxidation is demonstrated to be a promising reaction for sustainable hydrogen production by electrolysis but the hydroxyacid chemical structure plays a significant role in both electrochemical reactivity and selectivity.

SUPPORTING INFORMATION

Structure-reactivity effects of biomass-based hydroxyacids for sustainable electrochemical hydrogen production

Daniel Martín-Yerga[a,c]*, Jai White[a], Gunnar Henriksson[b], Ann Cornell[a]*

[a]*Department of Chemical Engineering, KTH Royal Institute of Technology, SE-100 44 Stockholm, Sweden*

[b]*Department of Fibre and Polymer Technology, KTH Royal Institute of Technology, SE-100 44 Stockholm, Sweden*

[c] Current address: *Department of Chemistry, University of Warwick, Coventry CV47AL, United Kingdom.*

*Corresponding authors e-mail:

D.M-Y daniel.martin-yerga@warwick.ac.uk

A. C amco@kth.se

SECTION 1. ADDITIONAL FIGURES

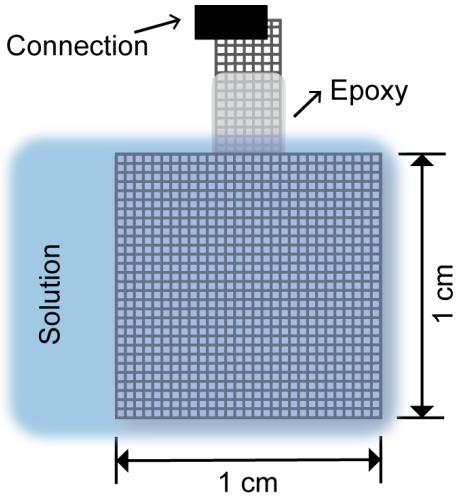

Figure S1. Schematic of the Ni foam electrode modified with epoxy coating to prevent electrolyte filling up the pores by capillarity and ensure a consistent and defined contact area.

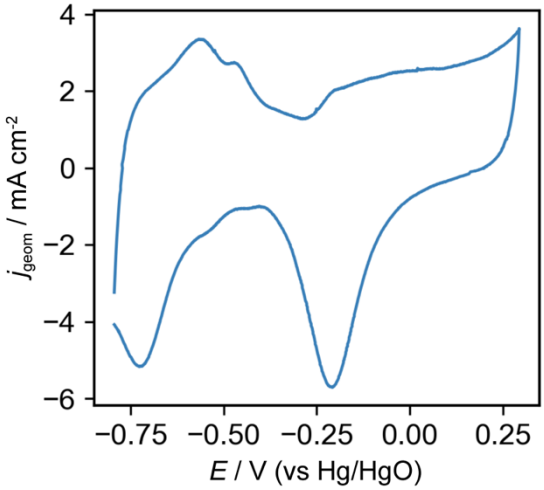

Figure S2. Cyclic voltammetry of the PdNi/Ni_{foam} electrode in 1 M NaOH solution employed to calculate the electrochemical surface area (ECSA), which was 143 ± 23 cm^2.

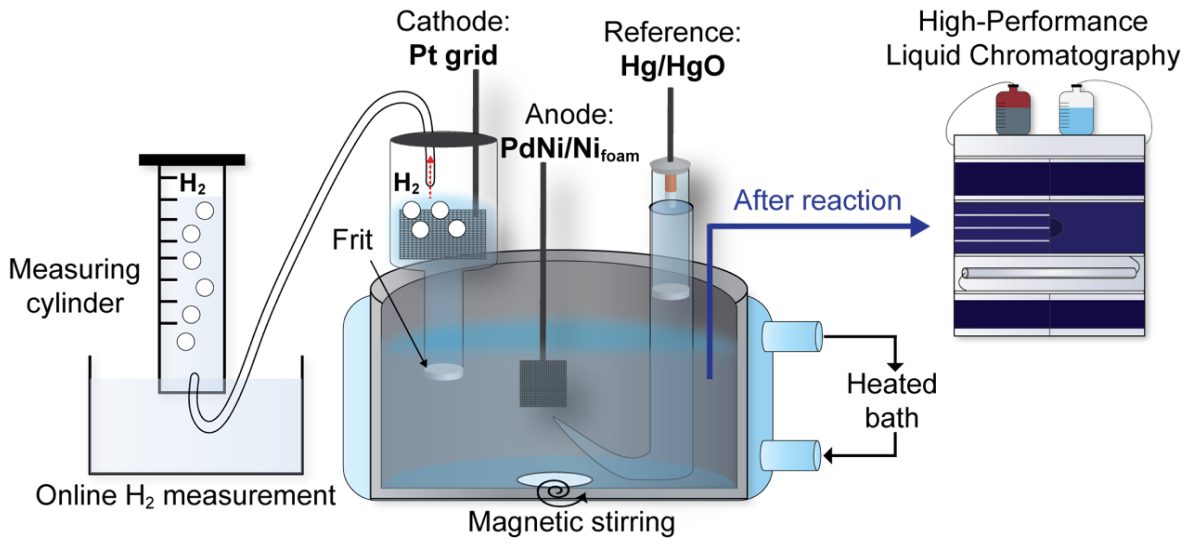

Figure S3. Schematic of the temperature-controlled electrochemical cell used for the hydroxyacids oxidation with separated cathodic and anodic compartments. The online H_2 measurement by gas displacement and the offline HPLC analysis are also depicted.

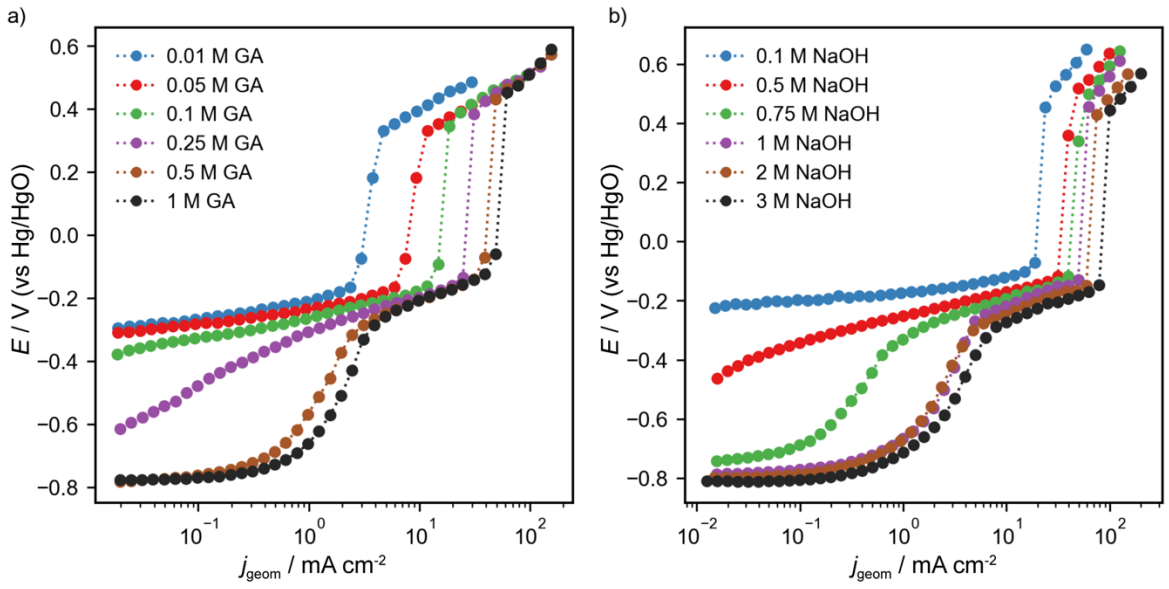

Figure S4. *iR*-corrected polarization curves for GA oxidation at different concentration of (a) GA in 1 M NaOH and b) NaOH in 0.5 M GA. Reaction temperature was 25 °C.

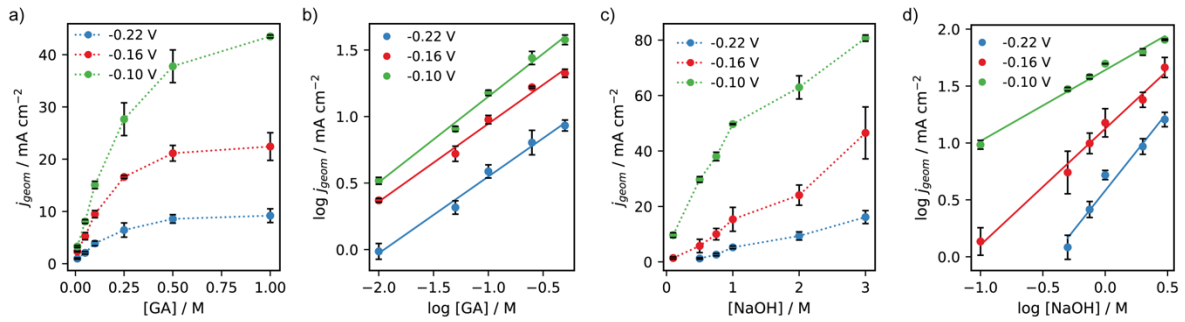

Figure S5. Dependence between the **(a)** current density and concentration of GA and **(b)** their logarithm representations at different potentials during the oxidation of GA in 1 M NaOH. Dependence between the **(c)** current density and concentration of NaOH and **(d)** their logarithm representations at different potentials during the oxidation of 0.5 M GA. Data was obtained from *iR*-corrected polarization curves as those shown in Figure S4. Standard deviations are calculated from n=3 experiments.

Kinetics information from the GA electrocatalytic reaction can be analysed by measuring the effect of reactant concentrations (GA and NaOH) on the current densities as previously reported for alcohol electrocatalytic oxidation.[1,2] Briefly, at steady-state conditions, the electrocatalytic current can be expressed as equation S1:

$$j = n\,F\,K_f C_{NaOH}^{a} C_{GA}^{b} \quad \textbf{(S1)}$$

where j is the current density, n is the number of electrons transferred in the reaction, F is the Faraday constant, K_f is the reaction rate constant, C_{NaOH} and C_{GA} are the concentrations of NaOH and gluconic acid in solution, respectively, and a and b are reactions orders with respect to NaOH and gluconic acid concentrations, respectively. When the electrode potential and the gluconic acid concentration are kept constant, equation S1 can be written in the form of equation S2:

$$\log j = A + a \log C_{NaOH} \quad \textbf{(S2)}$$

When the electrode potential and the NaOH concentration are kept constant, equation S1 can be written in the form of equation S3:

$$\log j = B + b \log C_{GA} \quad \textbf{(S3)}$$

From these equations representing $\log j$ vs $\log C_{\mathrm{NaOH}}$ or $\log C_{\mathrm{GA}}$ (as shown in Figure S5) can provide the reaction orders (a, b) respect to both reactant concentrations from the slope of the straight line. Reaction orders respect to NaOH (a) of 0.62, 1.02 and 1.39 and reaction orders respect to GA (b) of 0.59, 0.58 and 0.64 were calculated at different potentials of -0.10, -0.16 and -0.22 V, respectively. These results show the strong influence of the NaOH concentration on the GA electrocatalytic oxidation, and particularly at low potentials (near the onset of the reaction).

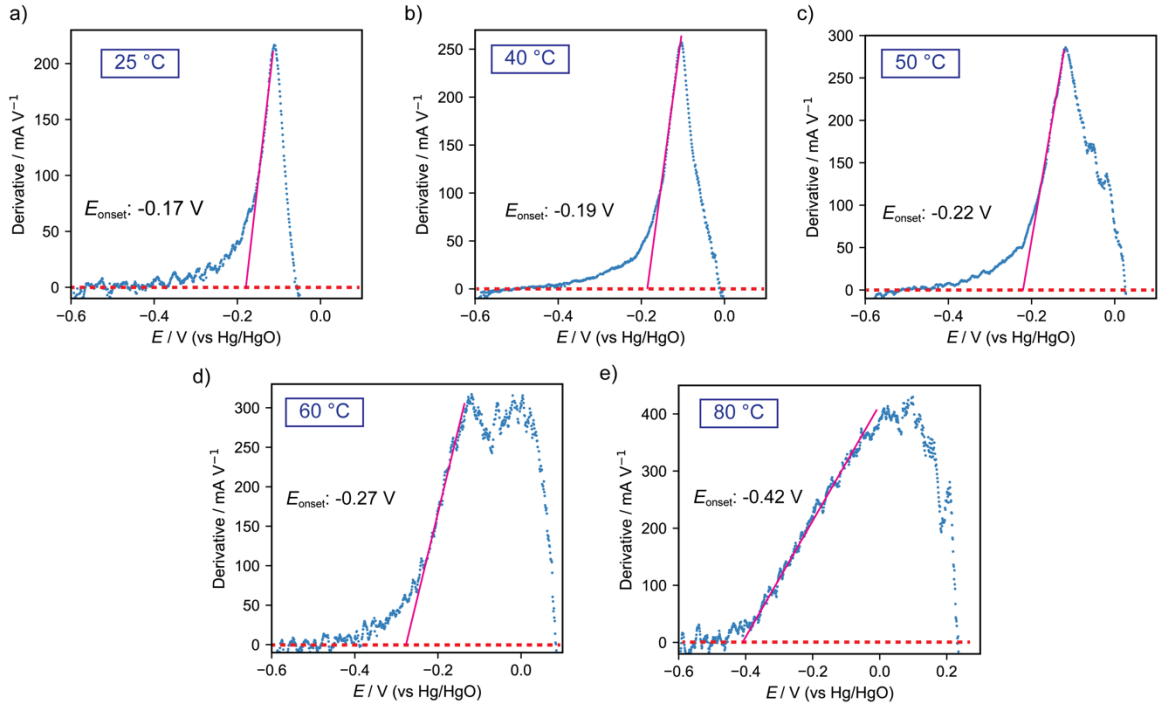

Figure S6. Voltammetric onset potentials for the oxidation of 2 M LA in 2 M NaOH at different temperatures. Scan rate was 10 mV s^{-1}.

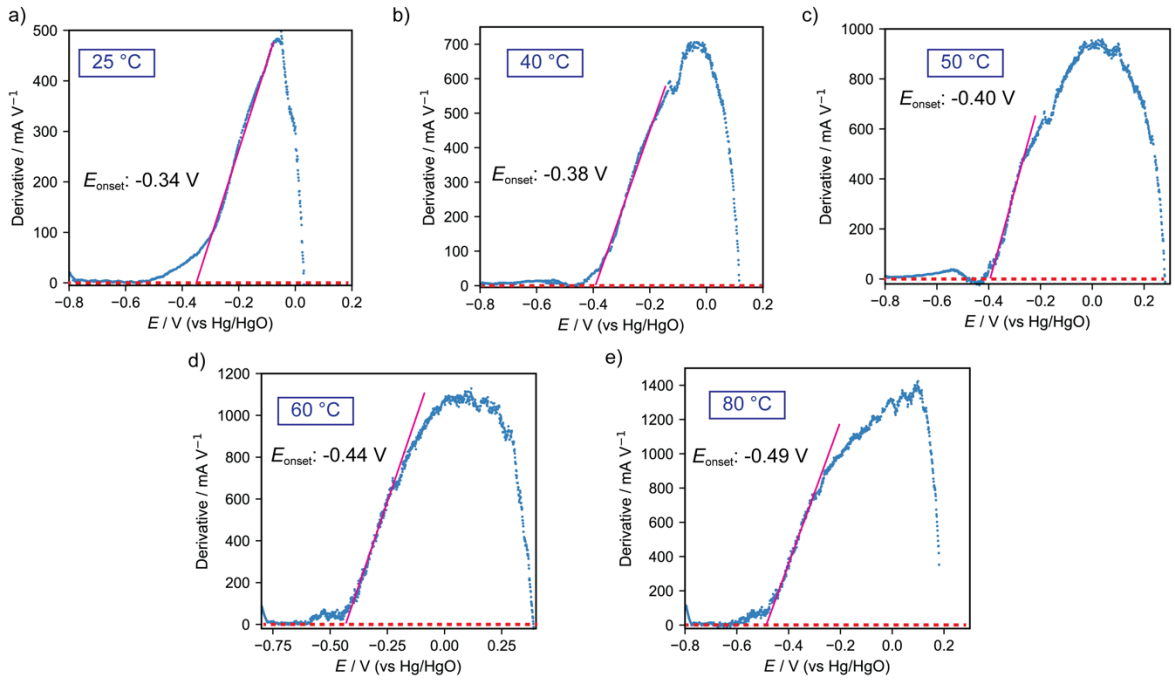

Figure S7. Voltammetric onset potentials for the oxidation of 0.5 M GA in 3 M NaOH at different temperatures. Scan rate was 10 mV s^{-1}.

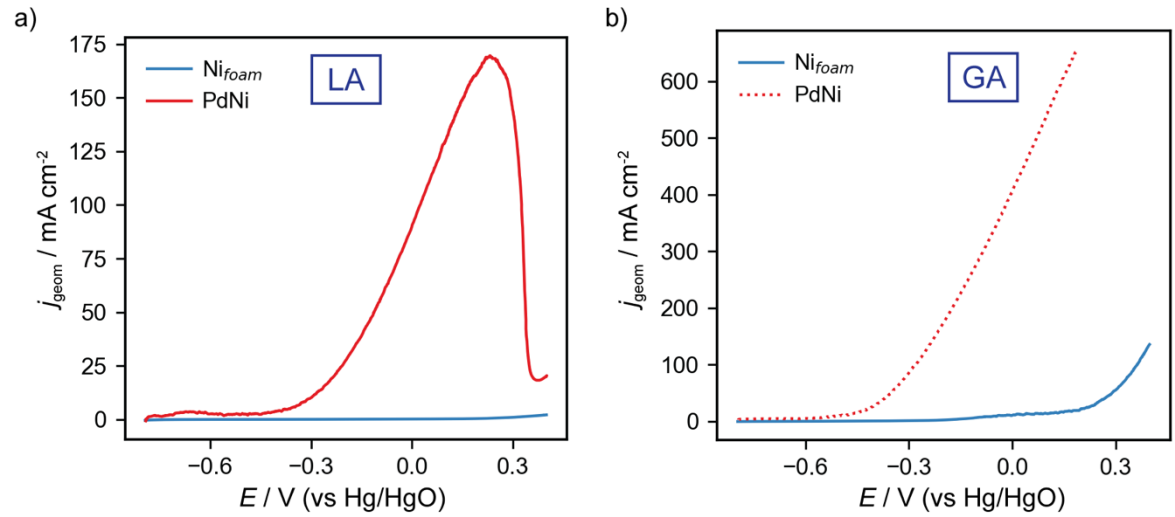

Figure S8. Linear sweep voltammogram for the oxidation of a) 2 M LA in 2 M NaOH and b) 0.5 M GA in 3 M NaOH at 80 °C on Ni foam (blue curves) and PdNi/Ni_{foam} (red curves) electrodes. Scan rate was 10 mV s^{-1}.

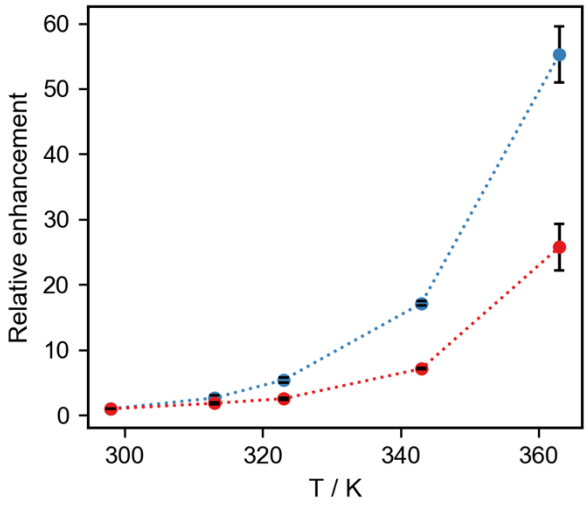

Figure S9. Relative enhancement of the current densities for LA and GA oxidation reactions at increasing temperatures. Data represented is at -0.15 V vs Hg/HgO for LA oxidation and -0.25 V vs Hg/HgO for GA oxidation. Data obtained from the *iR*-corrected polarization curves as shown in Figures 4c-d. Standard deviations are calculated from n=3 experiments.

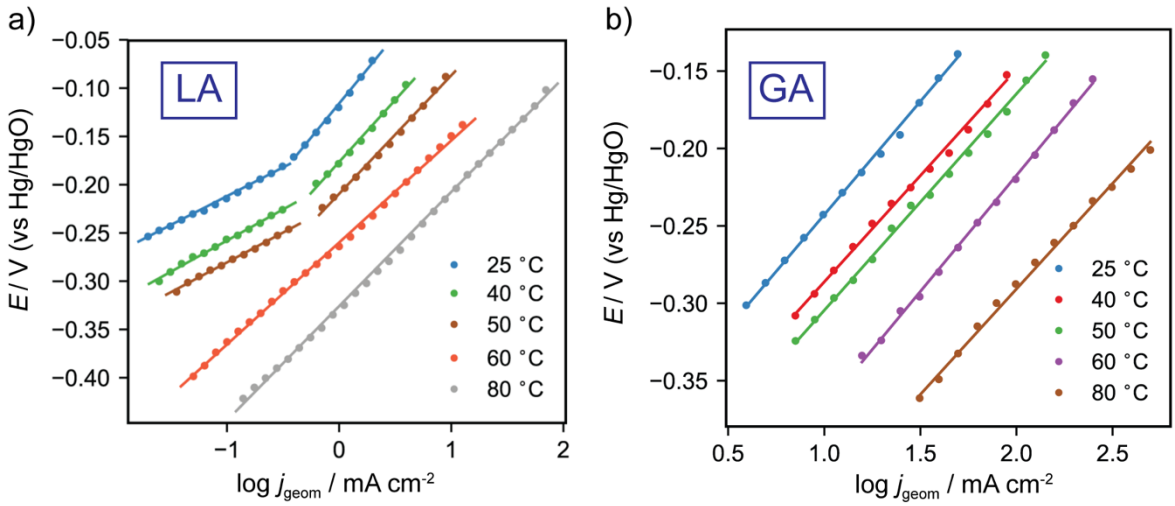

Figure S10. Representation of log *j* vs *E* at different reaction temperatures for the oxidation of a) 2 M LA in 2 M NaOH and b) 0.5 M GA in 3 M NaOH.

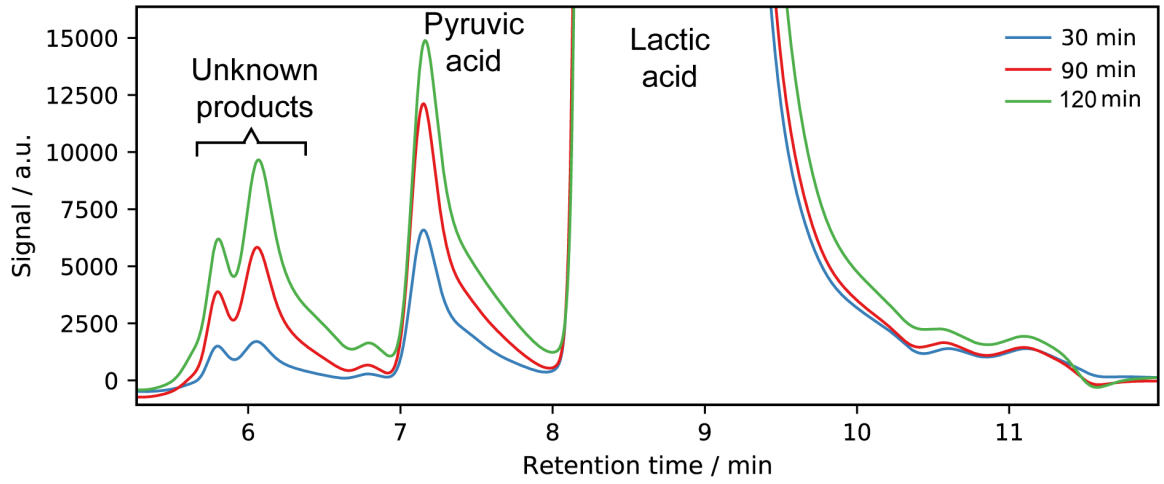

Figure S11. HPLC chromatogram for the liquid solution in the anodic compartment after the oxidation of 1 M LA in 1 M NaOH at 80 °C by applying 25 mA cm^{-2} at different reaction times (30, 60, 120 min).

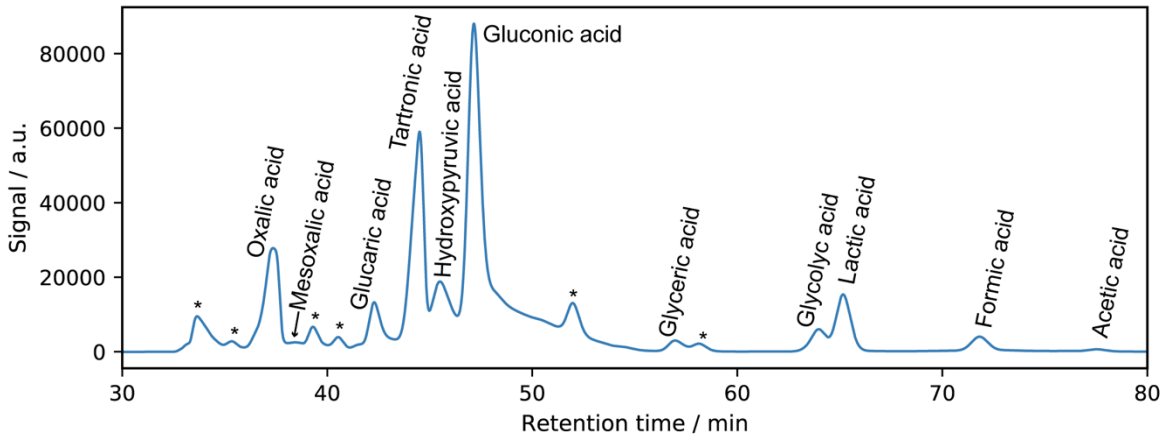

Figure S12. HPLC chromatogram for the liquid solution in the anodic compartment after the oxidation of 0.5 M GA in 3 M NaOH at 80 °C by applying 200 mA cm^{-2} for 2h. An asterisk represents a product that was not identified. Other chemicals evaluated by HPLC but not present in the product mixture were: glucuronic acid, glycolaldehyde, 5-ketogluconic acid, glyoxylic acid, succinic acid, pyruvic acid, tartaric acid, glyceraldehyde and dihydroxyacetone.

SECTION 2. CALCULATIONS OF SAVINGS IN ENERGY REQUIREMENT

The following equations were employed to calculate the savings in energy requirements for H_2 production ($\Delta\left(\frac{\text{kWh}}{\text{kg H}_2}\right)$) by replacing the anodic reaction from water oxidation to hydroxyacids oxidation:

$$\Delta\left(\frac{\text{kWh}}{\text{kg H}_2}\right) = \frac{\Delta P_{\text{anodic}}\ (\text{kW})}{\text{H}_2\text{ production rate }(\frac{\text{kg H}_2}{\text{h}})}$$

$$\Delta P_{\text{anodic}}\ (\text{kW}) = \frac{\Delta E_{\text{anodic}}\ (\text{V}) \times\ i\ (\text{A})}{1000}$$

$$\Delta E_{\text{anodic}}\ = E_{\text{anodic}}\ (\text{water oxidation}) -\ E_{\text{anodic}}\ (\text{hydroxyacid oxidation})$$

$$\text{H}_2\text{ production rate}\ \left(\frac{\text{kg H}_2}{\text{h}}\right) =\ \text{H}_2\text{ production rate}\ \left(\frac{\text{mol H}_2}{\text{s}}\right) \times \frac{3600\ \text{s}}{1\ \text{h}} \times \frac{1\ \text{kg H}_2}{496\ \text{mol H}_2}$$

$$\text{H}_2\text{ production rate}\ \left(\frac{\text{mol H}_2}{\text{s}}\right) = \frac{i\ (\text{A})}{F\ \left(\text{C}/_{\text{mol}}\right) \times z\ (\text{e}^-)}$$

where ΔP_{anodic} is the difference in power between the water and hydroxyacid oxidation reactions, calculated from the difference in anodic potentials (ΔE_{anodic}) at a specific current (i). The H_2 production rate was calculated through the Faraday's law of electrolysis considering a 100% faradaic efficiency and with $F = 96485$ C mol^{-1} (Faraday constant) and $z = 2$ e$^-$ transferred for the hydrogen evolution reaction.

SECTION 3. REFERENCES

[1] R. Jiang, D. T. Tran, J. P. McClure, D. Chu, *ACS Catal.* **2014**, *4*, 2577–2586.
[2] D. Chu, S. Gilman, *J. Electrochem. Soc.* **1996**, *143*, 1685–1690.